RSC Advances

ROYAL SOCIETY OF CHEMISTRY

www.rsc.org/advances

Pomelo peel as biomass-derived porous activated carbon is used for the preparation of a high energy density symmetric supercapacitor.

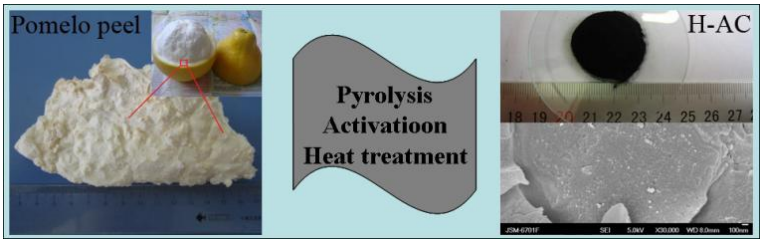

Journal Name

RSCPublishing

ARTICLE

Oxygen-enriched activated carbons from pomelo peel in high energy density supercapacitor

Cite this: DOI: 10.1039/xoxxoooooox

Chao Peng[b], Junwei Lang[a], Shan Xu[b]*, Xiaolai Wang[b]

Received ooth January 2012,
Accepted ooth January 2012

DOI: 10.1039/xoxxoooooox

www.rsc.org/

We used low-cost pomelo peel (PP) as biomass-derived porous activated carbon to fabricate a high energy density symmetric supercapacitor. The porous activated carbon was prepared from the pomelo peel (PP) via the pyrolysis and KOH activation process, followed by the heat treatment under argon atmosphere. The resulting porous carbon possesses very high specific surface area (2105 m^2/g) and abundant oxygen functionalities, which afford a wide voltage window of 1.7 V, the specific capacitance of 43.5 F/g and a high energy density of 17.1 Wh/kg for the as-assembled AC//AC symmetric supercapacitor. These impressive electrochemical characteristics may indicate the PP to act as a new biomass source of carbonaceous materials for low-cost and high performance electrical energy storage devices.

Introduction

The supercapacitor is one of the most promising energy storage devices due to its deliver high power within a very short period, simple cell configuration and excellent charge-discharge performance, compared with the rechargeable batteries and dielectric capacitors.[1,2] Porous activated carbon is a promising material for supercapacitors,[2] because of its numerous exceptional characteristics, including moderate costs, high thermal and chemical stability, hydrophobic surface properties, and high electrical conductivity. Studies have shown that in carbon-based supercapacitors, the high-surface area electrode is linearly proportional to capacitance, so to make carbon materials with high-surface area are crucial. To date, many physical and chemical activation methods, including chemical vapor deposition,[3] soft and hard template methods,[4-6] and chemical(KOH, CO_2, NH_3, and H_2O)-activation,[7-10] may the production of porous carbon with high surface areas (above 1000 m^2/g).

Recently, the use of biomass materials to produce porous activated carbon becomes of popular when business costs, wide availability, and energy/environmental concern are considered.[8] various biomass derived porous carbons, such as from fungi,[11] lignocellulosic materials,[12,13] corn grain,[14] celtuce leaves,[15] banana peel,[16] fish scales,[17] and starch,[18] have been reported. These materials have shown great potential as electrode materials for supercapacitors.

Pomelo belongs to citrus, grown in Southeast Asia and the south of the Yangtze River in the Chinese mainland. Pomelo is one of the very favourite fruit because of its fragrance, sweet, cool moist, nutrient-rich and high medicinal value. Whereas the pomelo peel is normally discarded.

In this paper, we used waste pomelo peels (PP) to prepare porous activated carbon by high-temperature carbonized and KOH activation as well as heat treatment under argon atmosphere. The resulting porous activated carbon shows an extremely high specific surface area of up to 2100 m^2/g as well as excellent energy density 17.1 Wh/kg. So we can believe that porous activated carbon derived from PP would be a promising material for high energy, power density and low cost supercapacitor. It is worth mentioning that a similar pomelo peel-derived activated carbon has been very recently reported by Shi et al.[19], in which the resulting carbon electrode also exhibits outstanding electrochemical properties, indicating that the potential applications of pomelo peel in energy storage may have been overlooked.

Experimental

Preparation of activated carbon

Pomelo peel (PP) was collected after people eaten pomelo off, and peeled out the exocuticle to remain, the as-obtained material was washed using deionized water and dried in a hot air oven at 60 ℃ for 48h. PP was pyrolysised in argon atmosphere and activated with the chemical etching agent of potassium hydroxide. Briefly, PP were carbonized at temperature of 600 ℃ for 2h in an argon flow of 40 sccm, and then obtained the carbonized carbon (denoted as P-C). Subsequently, KOH activation of the P-C was as follows: given mass of P-C was blended using KOH (KOH/P-C mass ratio 4), the mixtures were heated at 800 ℃ for 1h in a horizontal tube furnace with an argon flow of 40 sccm. The temperature was ramped from room temperature to 800 ℃ at 5℃/min. After cooling down in flowing argon flow to room temperature, the sample was neutralized by the 1 M HCl solution until a pH value of 7 was reached. Subsequently, as-obtained carbon material was transferred to the filter membrane, and using great amounts of Millipore water wash the sample for several times. Finally, the sample was dried at 60 ℃ in ambient for 10 h, which denoted as P-AC.

Furthermore process that the as-prepared P-AC sample was treated at 800 ℃ for 2h under argon atmosphere, which denoted as H-AC.

Structural characterization

The morphology and microstructure of the obtained activated carbon products were investigated using a field emission scanning electron microscope (FE-SEM, JSM-6701F). Crystallite structures were determined by a XRD (X' Pert Pro, Philips) using Cu Kα radiation from 5° to 90° . Nitrogen adsorption – desorption isotherm measurements were performed on a Micrometitics ASAP 2020 volumetric adsorption analyzer at 77 K. Before the experiments, both of activated carbon samples were adopted degassing process at 200 ℃ for 4h to eliminate the carbon particles surface contaminants. The Brunauer–Emmett–Teller (BET) method was utilized to calculate the specific surface area of each sample and the pore-size distribution was derived from the adsorption branch of the corresponding isotherm using the DFT method. The total pore volume was estimated from the amount adsorbed at a relative pressure of P/Po = 0.99. The surface chemical species of the P-AC and H-AC carbon materials were examined on a Perkin-Elmer PHI-5702 multifunctional X-ray photoelectron spectroscope (XPS, Physical Electronics, USA) using Al Kα radiation of 1486.6 eV as the excitation source. All the XPS spectra were calibrated by using Au $4f_{7/2}$ at 84.0 eV.

Electrode preparation and electrochemical measurements in a three-electrode system

The working electrodes were prepared following the method. Firstly, for the sake of coated the electroactive material in nickel gauze, as-produced material was grinded to powder. Subsequently, 80 wt. % of powder active material was mixed with 7.5 wt. % of acetylene black (>99.9%) and 7.5 wt. % of conducting graphite in an agate mortar until a homogeneous black powder was obtained. To this mixture, 5 wt. % of poly (tetrafluoroethylene) was added with a few drops of ethanol. After briefly allowing the solvent to evaporate, the resulting paste was coated in nickel gauze. The electrode assembly was dried for 16 h at 80℃ in air, and then was pressed at 10 MPa. Each carbon electrode contained about 8 mg of electroactive material for the electrochemical performance tests.

All the electrochemical measurements of each as-prepared electrode were carried out by an electrochemical working station (CHI660D, Shanghai, China) using a three-electrode system in 2 M KOH electrolyte at room temperature. A platinum sheet electrode and a saturated calomel electrode served as the counter electrode and the reference electrode, respectively. The cyclic voltammetry (CV) measurements were conducted at different sweep rates. Galvanostatic charge-discharge measurements were run on at different current densities. EIS analyses were recorded with using another electrochemical working station (Autolab, Switzerland) from 10 kHz to 0.1Hz with alternate current amplitude of 10 mV at open circuit potential and in 2 M KOH aqueous electrolyte.

Electrochemical measurements in two-electrode system

Symmetric supercapacitor (H-AC/H-AC supercapacitor) was fabricated. The electrodes were prepared by using nickel foam as the current collectors; each electrode contained 8 mg of electrochemical active material. The cathode and anode electrode were pressed together and separated by a porous nonwoven cloth separator. The electrochemical measurements of the symmetric supercapacitor were carried out in 1M $NaNO_3$ aqueous electrolyte using the electrochemical working station in a two-electrode cell at room temperature.

The specific capacitance of the supercapacitor cell can be evaluated from the charge-discharge test together with the following equation:

$$C_T(F/g) = \frac{I\Delta t}{\Delta E \times m}$$

Where I in A is the constant discharging current; Δt in s is the discharge time; ΔE in V is the potential window during the discharge process after IR drop; and m in g is the total mass of the two-electrode materials.

Specific energy density and power density are very important performance parameters of supercapacitor cell, which can be defined as follow:

$$E(Wh/kg) = \frac{0.5C_T V^2}{3.6}$$

$$P(W/kg) = \frac{E \times 3600}{t}$$

Where V in V is the voltage change during the discharge process after IR drop, and t in s is the discharge time.

Results and discussion

Structure and morphology

PP-based porous activated carbon materials were prepared according to the scheme of Fig. 1. In terms of shape in Fig. 2a, the isotherm of both carbon materials are found in accordance with the typical I of microporous materials according to IUPC classification, because the isotherm knees are sharp at low P/P_0 and the isotherm profiles completely overlap in the adsorption and desorption of nitrogen.[12-14] After the activation of P-C carbon, the value of BET surface areas and the total pore volume of P-AC increase from 5.7 to 2191 m^2/g and from 0.004 to 1.034 cm^3/g, respectively. Through H-AC carbon material was heat treatment, but the specific surface area of which still is 2057 m^2/g (see Table 1). As we know, as AC used on electrode material, the micropores are responsible for charges accumulation on the electrode–electrolyte interface whereas the small mesopores can play an adsorption and the transporting role for the electrolyte ions.[17] Fig. 2b shows the pore width distribution. There are two peaks at 0.86 nm and 1 nm can be found in micropore region corresponding to AC sample before and after heat treatment under the argon atmosphere, respectively. Both AC samples show virtually no pore width > 3 nm.

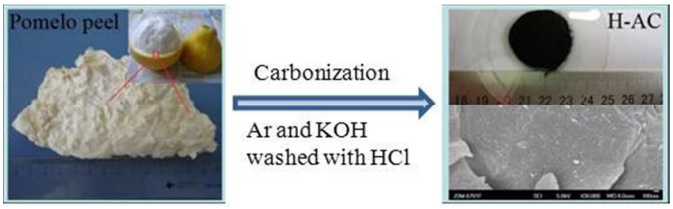

Fig. 1 The scheme of pomelo peel based activated carbon.

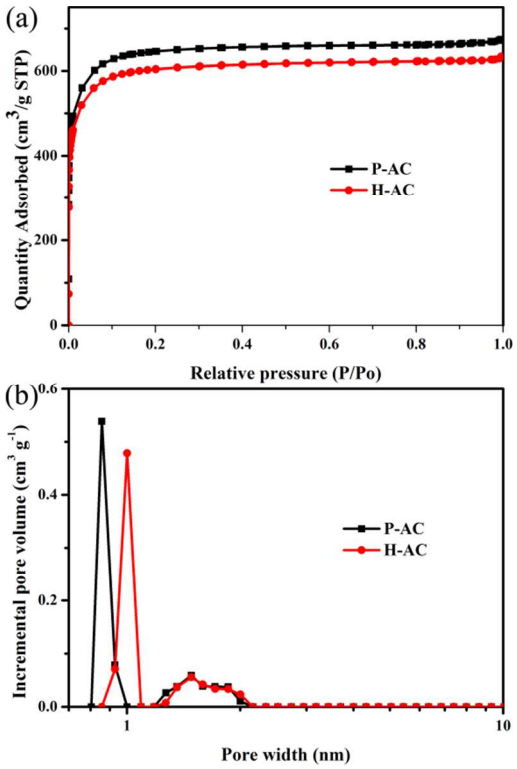

Fig. 2 (a) Isothermal curves of the as-prepared activated carbon derived from the pomelo peel with different treatment process; (b) DFT pore size distribution.

Table 1 Dates of BET measurements and the values of specific capacitance for the P-C, P-AC and H-AC carbon materials derived from the pomelo peel.

Samples	BET surface area (m^2/g)	Pore volume (cm^3/g)	Specific capacitance (F/g)
P-C	5.744	0.004	77
P-AC	2191	1.034	342
H-AC	2057	0.968	286

Fig. 3 shows the characteristics of powder XRD measurement of the three carbon materials. In the Fig. 3, two broad diffraction peaks at around 2θ = 23.3° and ~43°, respectively, which can be attributed to the (002) and (100) crystal plane diffraction peaks, indicating the presence of a low degree of graphitization, and graphite basal plane diffraction peak for P-C sample with amorphous carbon.[18,20] Both of them can be ascribed to the carbon structure with randomly oriented graphitic carbon layers.[21] After KOH activation, the intensity of (002) peak for P-C material has a significantly reduced and almost disappeared, but still retained the (100) peak. Considerable intensity in the low-angle scatter indicates the presence of a high density of pores for P-AC and H-AC carbon samples.[22,23]

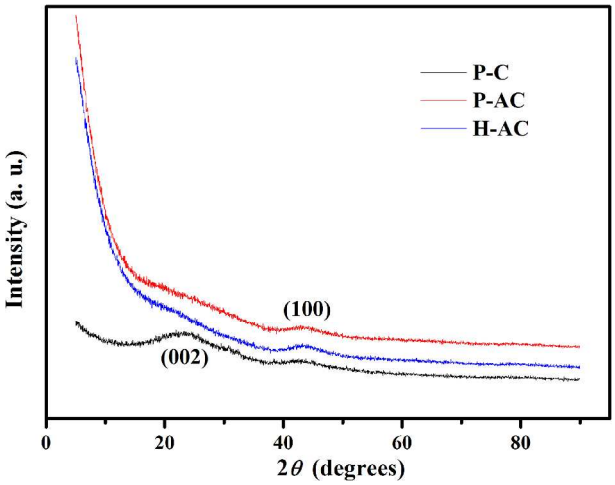

Fig. 3 XRD patterns of the P-C, P-AC and H-AC carbon materials.

In order to obtain the species and chemical states of the elements in the surface of the P- and H-AC activated carbon materials, X-ray photoemission spectroscopy (XPS) is carried out in Fig. 4. XPS spectra of the both carbon materials suggest the presence of two distinct peaks, which can be explained by existence of carbon and oxygen atoms. The C 1s peak of the P-AC was disassembled into four peaks, which corresponds to the signal of C=C-C bonds (284.7 eV), C-O bonds (286.3 eV), C=O bonds (287.7 eV) and O-C=O bonds (289.5 eV).[24-26] More detail dates were shown in table 2, considerable peak area of C-O bond; suggest a large amount of oxygen in the surface of P-AC sample. Compared with the C 1s XPS spectrum of P-AC, although the four components are still present in the H-AC carbon material, their areas undergo distinct changes. Briefly, the area of C=C-C and C=O bond are increased, but the area of C-O and O-C=O bond is decreased after heat treatment. These results demonstrate that heat treatment can significantly affect the amount of surface functionalities in the P-AC carbon materials. Factually, carbon materials with containing heteroatoms (such as oxygen- and nitrogen-enriched functional groups) have positive efforts on improving their electrochemical capacitive and voltage window shift.

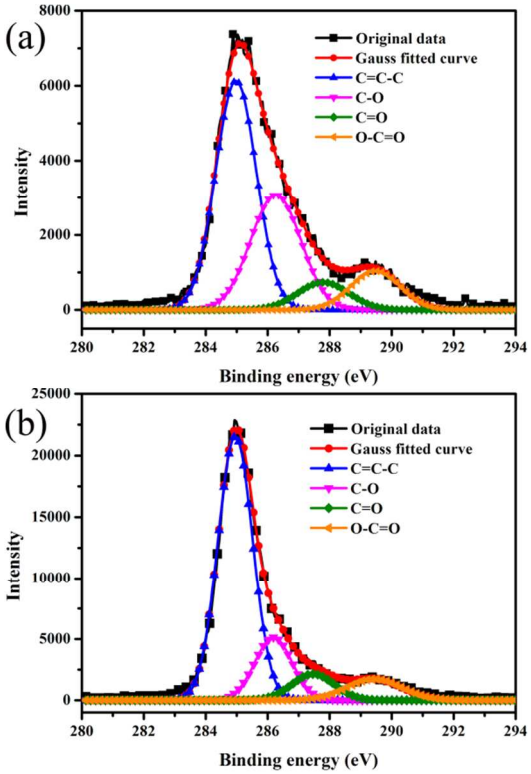

Fig. 4 The C 1s XPS spectra of activated carbon materials: (a) P-AC, (b) H-AC.

Table 2 Results of XPS surface characteristic for the P-AC and H-AC.

Sample	C at.%	O at.%	C=C-C at.% (284.7 eV)	C-O at.% (286.3 eV)	C=O at.% (287.7 eV)	O-C=O at.% (289.5 eV)
P-AC	84.72	15.28	51.09	31.01	7.55	10.35
H-AC	90.8	9.2	67.08	16.88	7.92	8.12

Fig. 5 shows the SEM photographs of P-C, P-AC and H-AC. Three carbon materials exhibit irregular and amorphous structure in the low magnification (Fig. 5a, c and e). While the surface of P-C sample displays a near-smooth surface except for a few holes in high-magnification image, which of P-AC material exhibits similar characters of particle-like and not smooth surface owing to the KOH etching under the high temperature activation. There is no significant change in the structure for the P-AC and H-AC carbon material after heat treatment at 800 ℃ for 2h under argon atmosphere, indication of only oxygen-contain functional groups was removed for the P-AC carbon material after heat treatment. For P-AC and H-AC electrodes with porous morphology and high surface area, which are the prime requirements in supercapacitor.

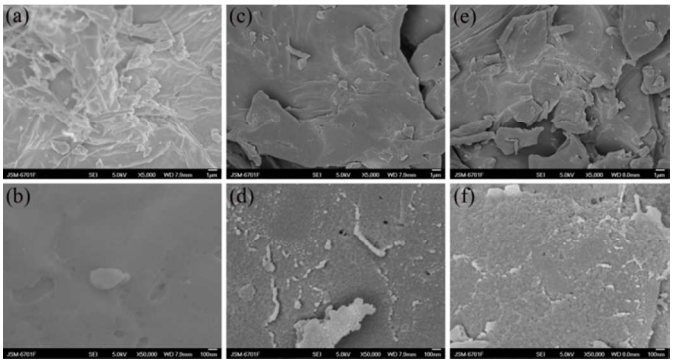

Fig. 5 SEM images of carbon materials for P-C, P-AC and H-AC: Low- (a, c and e) and high-magnification (b, d and f).

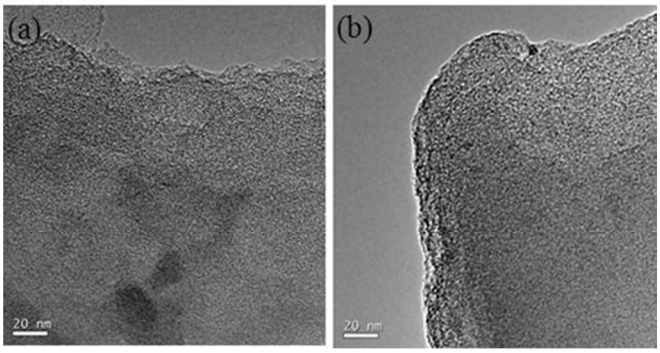

Fig.6 TEM images of carbon materials: (a) P-AC, (b) H-AC

Fig.6 shows the TEM photographs of P-AC and H-AC. It is easily to find that the microporous structure is very uniform, and no evident lattice fringe is found. There is no significant change in the structure for the P-AC and H-AC carbon material after heat treatment at 800 ℃ for 2h under argon atmosphere.

Electrochemical test for carbon electrodes in KOH aqueous electrolyte

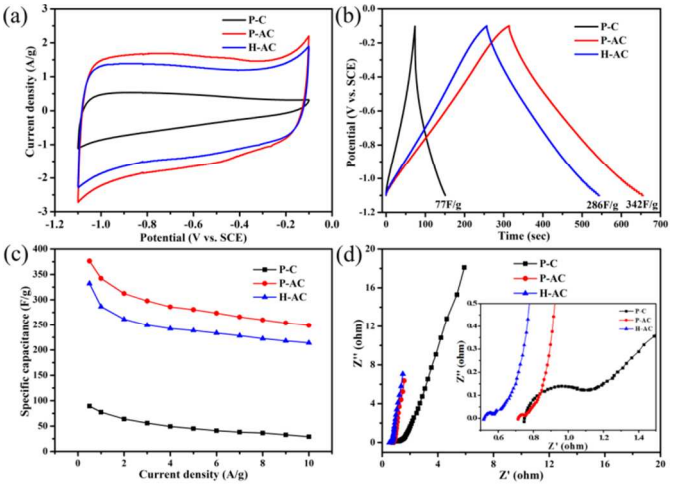

Fig. 7 Electrochemical performances test for the P-C, P- and H-AC samples in 2M KOH aqueous electrolyte at -1.1 to -0.1V under a three-electrode system. (a:CV curves at sweep rate of 5mV/s, b: GCD curves for at current density of 1A/g, c: Dependence of specific capacitance on discharge current density, d: Nyquist plot showing the imaginary part versus the

real part of impedance for these samples. Inset images show the dates of high frequency range.)

Fig. 7a shows the CV curves for the P-C, P- and H-AC electrodes in 2 M KOH aqueous electrolyte at sweep rate of 5 mV/s. From these curves, the shapes of P- and H-AC electrodes were closed to good rectangular, indicating of ideal capacitive for both of activated carbon materials with high specific surface area and microporous via KOH activation. Higher current density at the negative potential than at the positive potential for the CV curve of P-C electrode is attributed to the narrow porosity in the carbonized carbon derived from the PP.[27]

The charge-discharge curves of the P-C, P- and H-AC measured in 2M KOH at a current density of 1A/g in operating potential between -1.1 and -0.1V are shown in Fig. 7b. The values of specific capacitance for P-C, P- and H-AC electrodes are 77F/g, 342F/g and 286F/g, respectively, suggesting that the electrochemical capacitances of the X-AC are remarkably enhanced by the KOH activation. Longer discharge time of P-AC electrode than H-AC, which can be assumed to arise from enriched oxygen functionalities on the carbon surface, and obtained higher specific capacitance due to holding more surface charge.[28] Generally, well-shape triangles for the charge-discharge processes of P- and H-AC samples are suitable electroactive materials for supercapacitors.

Fig. 7c shows the change in the specific capacitance as a function of the discharge current density ranging from 0.5 to 10 A/g. The highest specific capacitance of 89.4 F/g, 376.3 F/g and 322.1 F/g for P-C, P- and H-AC electrodes were obtained at the current density of 0.5 A/g. When the current density as high as 10 A/g, the capacitance retention of these electrodes are 32.4%, 66.2% and 66.4%, respectively. The excellent capacitive behaviors confirmed that P- and H-AC carbon materials with oxygen-enriched surface and high specific surface area hold superior supercapacitve.

Fig. 7d shows the EIS analysis of P-C, P- and H-AC electrodes. The better electrochemical performance for P- and H-AC electrodes could be attributed to the better electronic conductivity compare with P-C, which can be seen from inset with high frequency of EIS. The internal resistance includes the total resistance of the ionic resistance of electrolyte, intrinsic resistance of active materials and contact resistance at the active material/current collector interface. The internal resistance of P-C, P- and H-AC electrodes are around 0.74, 0.72 and 0.52, respectively. We can conclude that low oxygen-containing carbon by heat treatment may improve the conductivity of the carbon materials. In Nyquist plot, it is obvious that the Warburg region of P- and H-AC electrodes are smaller than that of P-C carbon material, indicating that the P- and H-AC electrodes have little variation in ion diffusion path lengths and little obstruction of ion movement.[29] Furthermore, a nearly vertical line in the mid to low frequency confirmed that both P- and H-AC electrodes have excellent capacitive behavior.

Symmetric supercapacitor for H-AC material in $NaNO_3$ aqueous electrolyte

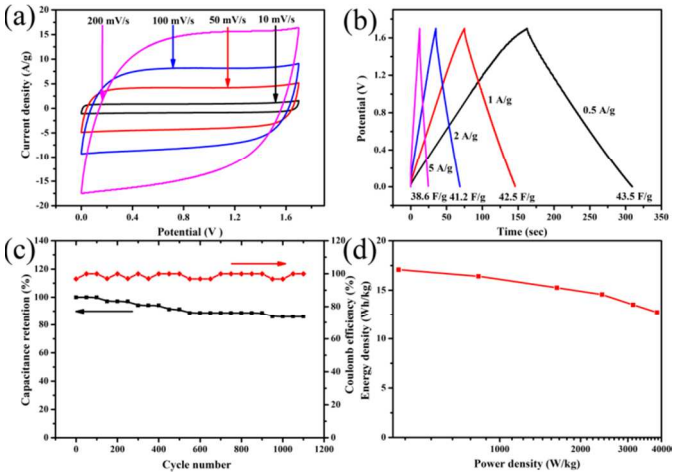

Fig. 8 Electrochemical performances tests for the H-AC(+)//H-AC(-) supercapacitors in 1 M $NaNO_3$ aqueous electrolyte at 0 to 1.7 V: (a) CV curves at different sweep rates; (b) GCD curves at different current densities; (c) Capacitance retention at the current density of 2 A/g after 1100 cycle numbers; (d) Ragone plot for cell capacitor.

A symmetric supercapacitor was fabricated with as-obtained H-AC carbon material to investigate its electrochemical capacitive in 1 M $NaNO_3$ aqueous electrolyte. The CV curves for the supercapacitor cell in at different sweep rates are shown in Fig. 8a. Observation form the CV curves, under the different sweep rates up to 200 mV/s, supercapacitor cell still displays a rectangular shape, ideal capacitive behavior and fast charge-discharge switching in the positive and negative elecltrodes, the result can be attributed to the unrestricted motion of electrolytes in the pores and a compact double-layer formation situation.[30,31]

Fig. 8b shows the charge-discharge curves of the cell supercapacitor in 1M $NaNO_3$ aqueous electrolyte for different current density in operating potential between 0 and 1.7V at various current densities from 0.5 to 5 A/g. Relative symmetric charge-discharge characteristic of well-shape triangular with ideal supercapacitive was displayed, which is another characteristic of an ideal capacitor. With the current density increasing, the specific capacitance decreased gradually. The result indicates that the electrode allows rapid ion diffusion and exhibits good electrochemical utilization. Compared with the specific capacitance of 43.5F/g at the current density of 0.5A/g, the specific capacitance of cell supercapacitor as high as 38.6F/g at the current density of 5A/g, so we can conclude this supercapapcitor cell has good discharge rate. The excellent results demonstrated as-assembled supercapaciror cell has superior capacitive behavior and discharge rate.

The excellent cycle stability of the H-AC (+) // H-AC (-) supercapacitor cell was demonstrated via running a constant current charge-discharge process. As shown in Fig. 8c, after charge-discharge the capacitors between 0 and 1.7 V during 1100 cycles at the current density of 2 A/g, it is about 90 % of the initial specific capacitances still is retained, indicating of the cell capacitors exhibit long-term cycle stability and good electrochemical reproducibility. Coulomb efficiency was calculated using following equation:[32,33]

$$\eta(\%) = \frac{T_d}{T_c} \times 100$$

Where Td and Tc are discharge time and charge time, respectively. The values of coulomb efficiency were calculated

and range from 96.8% to 100% during 1100 cycles for the symmetric supercapacitor.

The Ragone plot of the H-AC (+) / H-AC (-) supercapacitor cell was displayed in Fig. 8d. The symmetric supercapacitor cell fabricated with H-AC electrodes in $NaNO_3$ aqueous electrolyte presents a high energy density and power density. In addition, the operating voltage window of the supercapacitor can reach 1.7 V. Generally, the voltage window resulted from the stability window of the electrolyte. However, the nature of the electrochemical active materials also has an essential influence on the voltage shift. Enriched oxygen-containing in the H-AC carbon material provides a positive contribution to the voltage improve.[34] The symmetric supercapacitor H-AC (+) / H-AC (-) in this work, possess an energy density of 17.1 Wh/kg and a power density of 420 W/kg at discharge current density of 0.5 A/g. The power density increases to 3854 W/kg maintaining the energy density of 12.8 Wh/kg at a constant current of 5 A/g.

Conclusions

In summary, this paper successfully demonstrated porous activated carbon material with high specific surface area and oxygen-containing functionalities was prepared from the pomelo peel through pyrolysis and KOH activation, followed by heat treatment under the argon atmosphere. Operating potential window of as-fabricated symmetric supercapacitor can reach to 1.7 V. The maximum specific energy and specific power density of the supercapacitor cell reached 17.1 Wh/kg and 3854 W/kg, respectively. Meanwhile, P-AC and H-AC both exhibit superior electrochemical behavior in KOH aqueous electrolyte before and after heat treatment. These excellent results confirmed the applicability of pomelo peel derived carbon material and their promising as the electrode for the high energy density and low-cost supercapacitor.

Acknowledgements

This work was supported by the National Nature Science Foundations of China (21103205) and West Light Foundation of the Chinese Academy of Sciences (2013).

Notes and references

[a] State Key Laboratory for Oxo Synthesis and Selective Oxidation, Lanzhou Institute of Chemical Physics, Chinese Academy of Sciences, Lanzhou 730000, PR China

[b] Laboratory of Clean Energy Chemistry and Materials, Lanzhou Institute of Chemical Physics, Chinese of Academy of Sciences, Lanzhou, 730000, PR China

See DOI: 10.1039/b000000x/

1 L. Zhao, L. Z. Fan, M. Q. Zhou, H. Guan, S. Qiao, M. Antonietti and M.-M. Titirici, *Adv. Mater.* 2010, **22**, 5202–5206

2 Y. Zhai, Y. Dou, D. Zhao, P. F. Fulvio, R. T. Mayes and S. Dai, *Adv. Mater.* 2011, **23**, 4828–4850.

3 T. E. Rufford, D. Hulicova-Jurcakova, Z. Zhu and G. Q. Lu, *Electrochem. Commun,* 2008, **10**, 1594-1597.

4 W. Kim, J.B. Joo, N. Kim, S. Oh, P. Kim and J. Yi. *Carbon*, 2009, **47**, 1407-1411.

5 D. Hulicova-Jurcakova, M. Seredych, G. Q. Lu and T. J. Bandosz. *Adv. Func. Mater*. 2009, **19**, 438-447.

6 A. Elmouwahidi, Z. Zapata-Benabithe, F. Carrasco-Marín and C. Moreno-Castilla, *Bioresource Technology*, 2012, **111**, 185-190.

7 S. J. Han, Y. H. Kim, K.S. Kim and S. J. Park, *Current Applied Physics*, 2012, **12**, 1039-1044.

8 B. Xu, Y. Chen, G. Wei, G. Cao, H. Zhang and Y. Yang, *Materials Chemistry and Physics*, 2010, **124**, 504-509.

9 Y.K. Hsu, Y.C. Chen, Y.G. Lin, L.C. Chen and K.H. Chen, *Journal of Materials Chemistry*, 2012, **22**, 3383-3385.

10 Y. Wang, J. Cao, Y. Zhou, J.H. Ouyang, D. Jia and L. Guo, *Journal of the electrochemical society*, 2012, **159**, A579-A583.

11 M. P. Bichat, E. Raymundo-piñero and F. Béguin, *Carbon*, 2010, **48**, 4351-4361.

12 H.Y. Liu, K.P. Wang and H. Teng, *Carbon*, 2005, **43**, 559-566.

13 Y. A. Alhamed, H. S. Bamufleh, *Fuel* 2009, **88**,87-94.

14 K. S. W. Sing, D. H. Everett, R. A. W. Haul, L. Moscou , R. A. Pierotti , J. Rouquerol and T. Siemieniewska, *Pure Appl. Chem.* 1985, **57**, 603–619.

15 R.T. Wang, P.Y. Wang, X.B. Yan, J.W. Lang, C. Peng and Q.J. Xue. *ACS Applied materials & Interfaces,* 2012, **4**, 5800-5806.

16 Y. Lv, L. Gan, M. Liu, W. Xiong, Z. Xu, D. Zhu and D. S. Wright. *Journal of Power Sources* 2012, **209**,152– 157.

17 E. Frackowiak, G. Lota, J. Machnikowski, C. Vis-Guterl and F. Béguin, *Electrochimica Acta*, 2006, **51**, 2209-2214.

18 G.Q. Zhang, S.T. Zhang, *J Solid State Electrochem*, 2009, **13**, 887-893.

19 Q. Liang, L Ye, Z.H. Huang, Q. Xu, Y. Bai, F.Kang and Q.H. Yang. *Nanoscale*, 2014, DOI: 10.1039/C4NR04541F.

20 A. Jnes, H. Kurig and E. Lust, *Carbon*, 2007, **45**, 1226-1233.

21 T. Wang, S. Tan and C. Liang, *Carbon*, 2009, **47**, 1880-1883.

22 R. Vinodh, D. Sangeetha, *J Mater Sci.*, 2012, **47**, 852–859

23 Y. Zhu, S.Murali, M. D. Stoller, K. J. Ganesh, W. Cai, P.J. Ferreira, A. Pirkle, R. M. Wallace, K.A. Cychosz, M. Thommes, D. Su, E. A. Stach and R. S. Ruoff, *Science*, 2011, **332**, 1537-1541.

24 J. Chen, G. Zhang, B. Luo, D. Sun, X. Yan and Q.Xue, *Carbon*, 2011, **49**, 3141-3147.

25 J. Lang, X. Yan, W. Liu, R. Wang and Q.Xue, *Journal of Power Source*, 2012, **204**, 220-229.

26 G. Milczarek, A. Cizewski and I. Stepniak, *Journal of Power Source*, 2011, **196**, 7882-7885.

27 S.E. Chun, J. F. Whitacre, *Electrochimica Acta* 2012, **60**, 392-400.

28 G.Q. Zhang, S.T. Zhang, *J Solid State Electrochem*, 2009, **13**, 887-893.

29 K. Zhang, L.L. Zhang, X. S. Zhao, and J. Wu, *Chem. Mater.* 2010, **22**, 1392–1401

30 K.P. Wang, H. Teng, *Carbon*, 2006, **44**, 3218–3225

31 S.E. Chun, J.F. Whitacre, *Electrochimica Acta*, 2012, **60**, 392– 400

32 V.S. Jamadade, V.J. Fulari and C.D. Lokhande, *Journal of Alloys and Compounds*, 2011, **509**, 6257–6261.

33 S.G. Kandalkar, D.S. Dhawale, C.K. Kim and C.D. Lokhande, *Synthetic Metals* 2010, **160**, 1299–1302.

34 H. Zhu, X. Wang, F. Yang and X. Yang, *Adv. Mater.* 2011, **23**, 2745-2748.

